Available online at www.sciencedirect.com
ScienceDirect
Journal of Power Sources 168 (2007) 408–417
JOURNAL OF POWER SOURCES
www.elsevier.com/locate/jpowsour

# Niobium-clad 304L stainless steel PEMFC bipolar plate material Tensile and bend properties

Sung-Tae Hong, K. Scott Weil *

*Pacific Northwest National Laboratory, P.O. Box 999 Richland, WA 99352, United States*

Received 20 February 2007; accepted 12 March 2007
Available online 15 March 2007

**Abstract**

Niobium (Nb)-clad 304L stainless steel (SS) is currently under consideration for use as a bipolar plate material in polymer electrolyte membrane fuel cell (PEMFC) stacks. Because metal bipolar plates will likely be formed by stamping, the sheet-metal properties of this material were characterized in both the as-rolled and an optimized annealed condition via a series of bend and quasi-static tensile tests. Results from tensile testing demonstrate that annealing significantly softens and thereby improves the ductility of the material. Bend test results indicate that springback is nearly independent of the bend direction relative to rolling direction for both the as-rolled and annealed conditions. In the as-rolled condition, springback is also nearly independent of specimen orientation (i.e. whether the cladding layer is on the inside or outside of the bend). However, in the annealed condition, springback does depend on the cladding orientation relative to bending and was found in all cases to be substantially lower than that observed in the as-rolled condition. Microstructural analysis of the specimens indicates that two failure conditions can potentially arise, dependent on the thermomechanical condition of the material. In the as-rolled condition, failure initiates via fracture through the Nb cladding. In the annealed specimens, failure can occur by brittle fracture of an interfacial intermetallic layer that forms during the annealing treatment. This generates a series of crack-induced pores along the interface between the Nb cladding and the SS core, which eventually leads to ductile failure of the Nb cladding via localized necking. However, the conditions required for this phenomenon to take place are fairly extreme and can be readily avoided in practice. In general, the results suggest that to achieve acceptable stamping tolerances, the material should be annealed prior to forming and the bipolar plate flow channel pattern should be designed such that extreme levels of strain at the cladding/core interface are avoided to mitigate the potential for partial delamination within the material.
Published by Elsevier B.V.

*Keywords:* Clad sheet; Bipolar plate; Proton exchange membrane fuel cell; Bend test

## 1. Introduction

Despite significant technical progress made in recent years toward developing a commercially viable polymer electrolyte membrane fuel cell (PEMFC) system, the device currently finds commercial use in only niche applications [1]. Among the reasons for this are, the high cost of PEMFC stack manufacture and the steady loss in power output typically observed during long-term, continuous operation [2]. According to a recent assessment of PEMFC technology by the U.S. Department of Energy, "Fuel cells are currently five times more expensive than internal combustion engines and do not maintain performance over the full useful life of the vehicle [3]." Additional factors hindering the acceptance of PEMFCs in transportation markets are their current size and weight [4], which limit the specific power that can be generated. For this technology to be competitive, cost reduction and performance improvement must come from all aspects of PEMFC system design and manufacture.

One of the most bulky components in the stack with respect to both weight and volume is the bipolar plate. In addition, it is one of the most expensive to manufacture. This component serves not only as the electrical junction between serially connected cells in the stack, but also performs several other key functions in the overall device, including [5]: distribute fuel and oxidant uniformly over the active areas of the cells; facilitate water management of the membrane to keep it humidified, yet mitigate flooding; act as an impermeable barrier between the fuel and oxidant streams (particularly $H_2$) to maintain the hydrogen gradient across the membrane necessary for high power output; provide structural support for the stack; and remove heat

* Corresponding author. Tel.: +1 509 375 6796; fax: +1 509 375 4448.
*E-mail address:* scott.weil@pnl.gov (K.S. Weil).

0378-7753/$ – see front matter. Published by Elsevier B.V.
doi:10.1016/j.jpowsour.2007.03.032

Table 1
Thicknesses of Nb and SS used in cold roll bonding

| Materials | Thickness prior to rolling (mm) | | Total thickness after final rolling (mm) | Total nominal thickness strain |
|---|---|---|---|---|
| | Nb | SS | | |
| 5Nb-clad 304L SS | 1.27 | 24.13 | 0.254 | −0.99 |
| 10Nb-clad 304L SS | 1.32 | 11.88 | 0.254 | −0.98 |

from the active areas of the cells. While various materials have been considered for use in this component [6–11], metals offer a number of intriguing design advantages particularly for automotive stack applications, including: low-cost, mass-production via stamping or embossing of sheet product; fabrication in very thin form (<150 μm) to reduce weight and volume in the overall stack; impermeability to fuel, oxidant and water vapor; and in general, excellent thermal conduction properties and good mechanical robustness. However, a potential show-stopper with any metal-based PEMFC stack component is surface corrosion, and the current drive to increase the operating temperature of the stack will only exacerbate this problem. Corrosion of the bipolar plate leads to a release of metal ions that can contaminate the electrolyte membrane and poison the electrode catalysts, thereby exaggerating the long-term degradation issues with PEMFC stacks. In addition, the formation of a passivating oxide or oxyhydroxide layer on the surface of the metal tends to increase the contact resistance between the bipolar plate and the adjacent carbon gas diffusion layer, often by many orders of magnitude, which both limits the amount of power that can be generated by the stack and serves as an additional source of heat that must be removed during operation.

Various schemes have been investigated for protecting metallic bipolar plates, most of which rely on a thin, inert yet electrically conductive coating such as diamond-like carbon or titanium nitride [12–14]. However, there are a number of practical problems with deploying a surface coating strategy, including the unintended incorporation of flaws during processing, concerns with handling damage (chipping and scratching) during subsequent manufacturing steps, poor adhesion between the coating and underlying substrate during stack assembly, and the additional costs associated with the coating process. Desirable is a bipolar plate material that incorporates the advantages of metal, but undergoes little or no corrosion and is not susceptible to the manufacturing issues associated with coatings.

Recently, we reported on the electrochemical properties of niobium-clad stainless steel (Nb-clad SS) for potential use in a new clad PEMFC bipolar plate material concept [15]. Test results demonstrated that the concept is electrochemically viable, i.e. it affords excellent corrosion stability under an accelerated version of simulated stack conditions, while allowing material costs to be minimized by incorporating the passivating Nb as a thin layer roll clad to a more robust steel sheet. To date, testing has been conducted only on as-rolled, flat samples; the work needs to be validated on material in an as-formed condition that is representative of a prototypic metal PEMFC bipolar plate. Prior to this, the forming properties of the material must be evaluated. For example, a common technique currently employed in the manufacture of both PEMFC and solid oxide fuel cell (SOFC) monolithic metal components is progressive stamping. However, there are a number of sheet-metal properties that must be characterized before considering the Nb-clad material for bipolar plate design and subsequent fabrication via stamping, including yield stress, elongation, anisotropy, residual stress, formability, and springback [16]. Presented here is an initial evaluation of the tensile and bend properties of the Nb-clad SS material currently under consideration for PEMFC stack application.

## 2. Experimental set-up

The characterization studies were conducted on Nb-clad 304L SS sheets fabricated via roll bonding by Engineered Materials Solutions Inc. (EMS; Waltham, MA). As listed in Table 1, two different ratios of Nb to SS and two different thermomechanical conditions, as-rolled and annealed, were investigated. Annealing was conducted in high vacuum at 982 °C (1800 °F) for 15 min at EMS. Prior to characterization, the sheets were degreased by ultrasonically cleaning in acetone and methanol followed by rinsing with distilled water.

Specimens used in quasi-static tensile tests were cut from the clad metal sheets along three different angles to the direction of roll bonding, $\theta = 0^\circ$, 45° and 90°, as schematically shown in Fig. 1. The tests were performed according to the ASTM E8-04 [17] using an MTS universal test machine. During testing, the specimens were loaded in tension at a constant strain rate of 0.05 $min^{-1}$ (under a strain controlled condition) to the point of rupture. A calibrated load cell and extensometer were used, respectively, to record changes in the applied tensile force and the length of the specimen during each test.

Bend tests were conducted according to the ASTM E290-97a [18] for three-point bending using specimens measuring 57 mm in length and 20 mm in width. The specimens were cut from the clad metal sheets along two different angles to the rolling direction, $\theta = 0^\circ$ and 90°. In addition, the specimens were tested

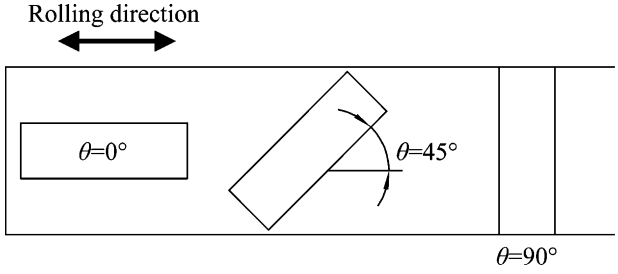


Fig. 1. A schematic of the specimen preparation direction with respect to the rolling direction.

under two different orientations with respect to the Nb cladding, i.e. with the Nb facing outward to the bend (denoted as Nb-out) and the Nb facing inward to the bend (denoted as Nb-in). Shown in Fig. 2(a) is a schematic of the experimental set-up for the tests. The distance between the supports, $C$, is defined by the ASTM E290-97a as:

$$C = 2r + 3t \pm 0.5t \quad (1)$$

where $r$ is the radius of the mandrel and supporting rollers and $t$ is the thickness of the sheet specimen. The distance $C$ was selected to be $C = 2r + 3.5t$ in this investigation.

Testing was performed by applying a vertical force $F$ via the mandrel midway between the two supports. This force and the vertical displacement $h$ of the mandrel were recorded as a function of time, respectively, using a calibrated load cell and LVDT. As seen in Fig. 2(a), a half bend angle $\alpha/2$ forms between each leg of the specimen and the horizontal reference axis. Thus for the dimensions of a given test fixture there is a maximum bend angle that can be achieved, which is defined as the operation limit angle, $\alpha_L$.

During initial testing, the specimens were bent to two different bend angles $\alpha = \alpha_L/2$ and $\alpha_L$ in the three-point bend test fixtures. To achieve a third bend angle of $\alpha = 180^\circ$, the specimens bent to $\alpha = \alpha_L$ were further deformed by applying force against the ends of the specimen with a spacer inserted within the bend, as schematically shown in Fig. 2(b). As specified by ASTM E290-97a, the thickness of the spacer was equal to twice the radius of the mandrel in the three-point bend test [18]. Finally an extreme version of bend testing, a flattening test [18], was conducted to investigate potential failure mechanisms in the materials. This test was performed by placing specimens bent to $\alpha = 180^\circ$ between two parallel platens and pressing to a vertical force per unit width of, $F/w$, of 60 kN m$^{-1}$, as schematically shown in Fig. 2(c).

In the present investigation two test fixtures were employed, each with a different mandrel radius. Listed in Table 2 are the radii of the mandrels and the corresponding distances between the supports and the operation limit angles. The amount of springback in the bent specimens [i.e. the tendency to partially return to the original shape because of the elastic recovery [19] or $\Delta\alpha$, as defined in Fig. 2(d)] was determined by comparing the maximum bend angle achieved during testing to that measured in the specimen after removal from the test fixture. To measure the repeatability of the test, twenty annealed 5Nb-clad SS specimens (10 in the Nb-out orientation and 10 in the Nb-in orientation) were bent to $\alpha = \alpha_L$ with $r = 6.4$ mm. The standard deviations of the springback angles in this series of experiments were found to be 1.4 and 1.5% of the mean value of the results for Nb-out and Nb-in orientations, respectively. Given the high degree of repeatability, it was decided that only three specimens

Table 2
Experimental parameters employed in three-point bend testing

| $r$ (mm) | $C$ (mm) | $\alpha_L$ (°) |
|---|---|---|
| 3.2 | 7.3 | 124 |
| 6.4 | 13.7 | 144 |

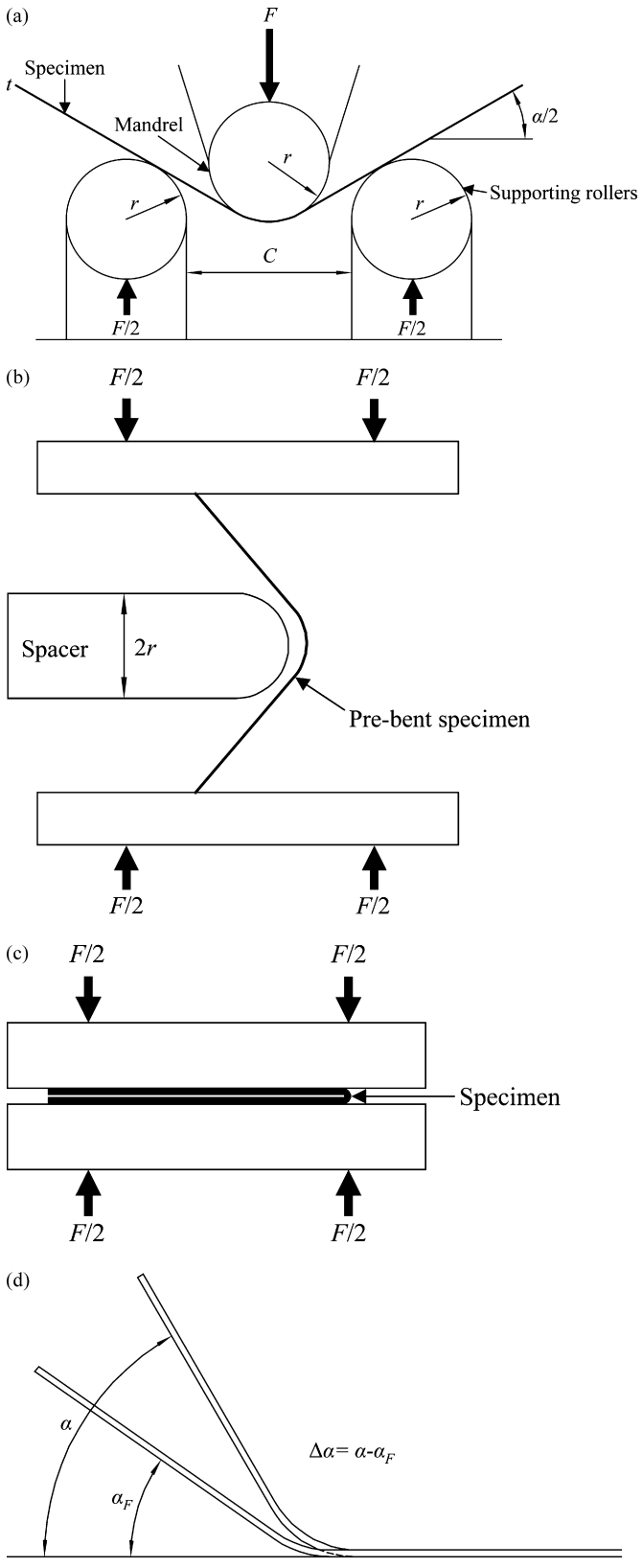


Fig. 2. Schematic of the experimental set-ups employed in: (a) the three-point bend tests, (b) the 180° bend tests, and (c) the flattening tests. (d) A schematic of springback in a bent specimen.

were needed to characterize each material condition in subsequent bend testing, with the mean value of $\Delta\alpha$ reported for each group in the final analysis.

Microstructural analysis of the clad metal specimens prior to and after bend testing was conducted on planar and polished cross-sectioned samples using an Axiovert-25 optical microscope and a JEOL JSM-5900LV scanning electron microscope (SEM) equipped with an Oxford energy dispersive X-ray analysis (EDX) system that employs a windowless detector for quantitative detection of both light and heavy elements. In order to avoid electrical charging on the samples, they were gold coated and grounded. Elemental profiles were determined across the joint interfaces in the line-scan mode.

## 3. Results

### 3.1. Tensile properties

Shown in Fig. 3(a and b) are the nominal stress–strain curves of the as-rolled and annealed 10Nb-clad SS material

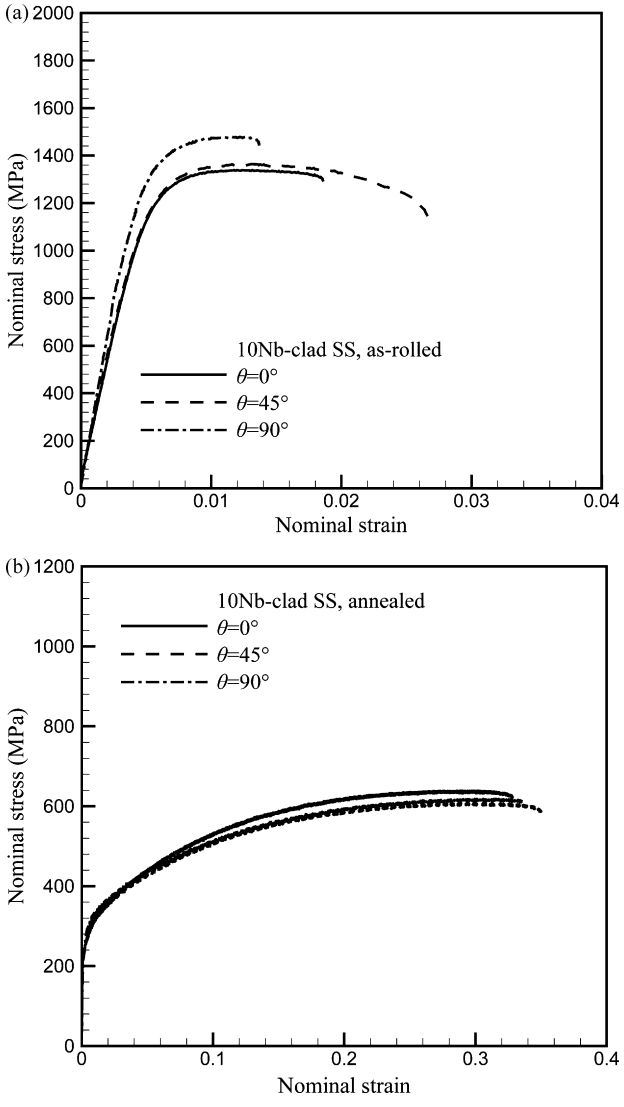


Fig. 3. Stress–strain curves of the 10Nb-clad SS specimens in: (a) the as-rolled condition and (b) the annealed condition.

Table 3
Effective mechanical properties of the 5Nb- and 10Nb-clad 304L SS sheet materials in the as-rolled and annealed conditions

| Material | Heat treatment | $\theta$ | Elastic modulus (GPa) | 0.2% yield stress (MPa) | Stain hardening exponent | Ultimate tensile strength (MPa) | Uniform elongation (%) | Total elongation (%) | $R$ |
|---|---|---|---|---|---|---|---|---|---|
| 5Nb-clad 304L SS | As-rolled | 0 | 287.6 | 1457.3 | N/A | 1472.7 | 0.95 | 2.13 | 0.38 |
| | | 45 | 320.9 | 1338.7 | N/A | 1407.6 | 1.02 | 1.09 | 0.89 |
| | | 90 | 299.4 | 1443.3 | N/A | 1539.3 | 1.56 | 2.68 | 0.31 |
| | Annealed | 0 | 302.3 | 205.5 | 0.246 | 597.9 | 27.91 | 31.80 | 0.07 |
| | | 45 | 292.6 | 242.8 | 0.246 | 631.9 | 27.94 | 30.93 | 1.78 |
| | | 90 | 312.7 | 257.7 | 0.278 | 647.4 | 32.07 | 38.85 | 2.22 |
| 10Nb-clad 304L SS | As-rolled | 0 | 241.1 | 1284.2 | N/A | 1338.1 | 1.18 | 1.79 | 0.67 |
| | | 45 | 240.4 | 1309.1 | N/A | 1364.2 | 1.30 | 2.69 | 1.21 |
| | | 90 | 258.4 | 1401.5 | N/A | 1477.5 | 1.16 | 1.26 | 1.83 |
| | Annealed | 0 | 271.8 | 253.7 | 0.259 | 638.2 | 29.62 | 33.10 | 1.39 |
| | | 45 | 233.4 | 251.3 | 0.259 | 609 | 29.63 | 35.35 | 1.28 |
| | | 90 | 262.5 | 272.8 | 0.273 | 618.1 | 31.49 | 34.38 | 1.36 |

as tested along, 45° to, and perpendicular to the direction of rolling ($\theta = 0°$, 45° and 90°, respectively). The shapes of the stress–strain curves for the 5Nb-clad SS material in the as-rolled condition and annealed conditions were found to be quite similar to those of the 10Nb-clad SS in the as-rolled condition and annealed conditions, respectively. Data from all 12 tests are summarized in Table 3. Also listed are the anisotropy parameters $R_\theta$ ($\theta = 0°$, 45° and 90°) for each material/thermomechanical condition, where $R_\theta = 1$ denotes isotropy in the material. Note that the strain hardening exponent, $n$, is calculated only for the specimens which do not contain the effect of work hardening [20]. As anticipated, the results indicate that annealing significantly improves ductility and softens the Nb-clad SS material by allowing it to thermally recover from the cold worked state of the as-rolled condition. $R_\theta$ values of 1–2 are not surprising given that stainless steel makes up 90–95 (v/o) of the clad material and an average anisotropy parameter for stainless steel ranges from 1.3 to 1.8 [19]. In general, the annealed 10Nb-clad material displays a slightly improved set of elongation and strength properties relative to the annealed 5Nb-clad material (~10% higher in both cases). The two as-rolled materials exhibit elongations that are likely too low for practical use in the PEMFC bipolar plate application.

### 3.2. Bend properties

Results from bend testing also demonstrate the significant effect of annealing on the mechanical properties of the Nb-clad SS materials. An example is given in Fig. 4, in which plots of vertical load per unit width, $F/w$, up to $\alpha = 0.5\,\alpha_L$ are shown as a function of mandrel displacement for the as-rolled and annealed 10Nb-clad SS specimens (for $r = 3.2$ mm and $\theta = 90°$). As seen in Fig. 4, the annealed specimens display significantly softer behavior than specimens in the as-rolled condition. The same

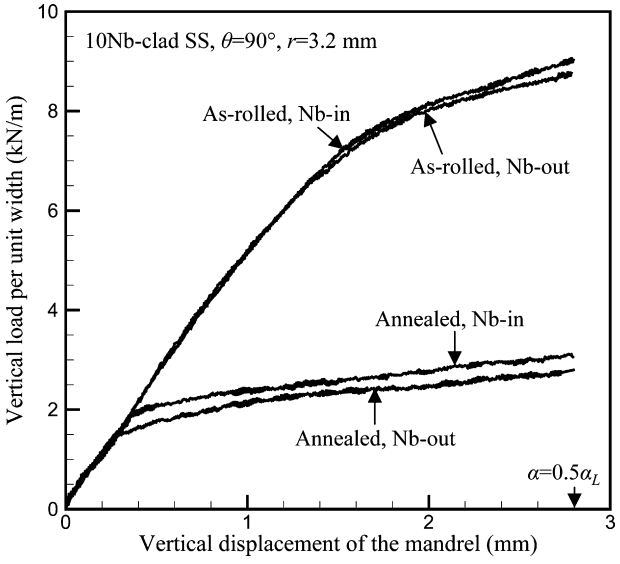


Fig. 4. The histories of the vertical load per unit width up to $\alpha = 0.5\,\alpha_L$ as a function of the vertical displacement (positive in downward direction) of the mandrel for the as-rolled and annealed 10Nb-clad SS specimens ($r = 3.2$ mm and $\theta = 90°$).

trend is observed in the springback data. Plotted in Fig. 5(a–d) are measurements of the springback angle $\Delta\alpha$ as a function of the bend angle $\alpha$ for the four material conditions studied. A quick comparison of the results obtained for the as-rolled and annealed conditions of each material type shows that springback is significantly reduced by annealing. Interestingly, in the as-rolled condition there is little effect of specimen orientation (Nb-in versus Nb-out) or the angle $\theta$ between the bend and rolling directions on the bend properties of either clad material. While $\theta$ also has little effect on springback in the annealed specimens, material orientation plays a significant role.

In a work-hardening material, the degree of springback depends approximately on two factors: the elastic modulus of the material and the induced flow stress [20]. Therefore, the lack of dependency of springback on $\theta$ observed in for the as-rolled specimens in Fig. 5(a and c) is reasonable, since elastic modulus is independent of thermomechanical condition and the yield strengths of comparable specimens tested under the three values of $\theta$ are not significantly different, as seen in Table 3. Similarly, the degree of springback is approximately constant for the annealed specimens, regardless of $\theta$.

However, note that once the SS core has been softened via heat treatment, material asymmetry (i.e. material orientation in the bend test) exerts an appreciable effect on springback. Conversely, springback in the as-rolled material is independent of material orientation. The difference in behavior can be attributed to the state of work hardening in the SS core. During rolling the 304L SS undergoes a greater degree of hardening than the Nb cladding, based on the strain hardening parameters of each material [21]. As a result, the thick, hardened core dominates the clad material's mechanical response in bending, relative to the far thinner, metallurgically softer cladding layer. When the original non-hardened state of the clad is recovered by annealing, flow stresses in both constituent materials are low. Upon bending, the two materials are strained and eventually the flow stresses in both build as they undergo plastic deformation. In this way, the location of the cladding layer during bend testing (i.e. on the inner radius or outer radius of the bend) affects the amount of strain and therefore flow stress in the niobium. This subsequently impacts the degree of springback measured in the overall clad material.

### 3.3. Microstructural analysis

Cross-sectional back scattered electron images of the as-rolled and annealed 10Nb-clad SS materials are shown, respectively, in Fig. 6(a and b). It is apparent from Fig. 6(a) that roll bonding yields a metallurgical bond between the cladding and underlying core evidenced by a non-diffuse interface and no interfacial porosity. For the as-rolled Nb-clad SS material, only a few intermetallic phase inclusions were observed along the interface. Results from EDX characterization demonstrate only a minor amount of iron diffusion into the niobium cladding during rolling. Spot chemical analyses at the points indicated in Fig. 6(a) are provided in Table 4. As listed in Table 4, diffusion is limited to a ~1 μm thick region on either side of the bondline. However, Fig. 6(b) shows that in the vacuum annealed specimen a micron

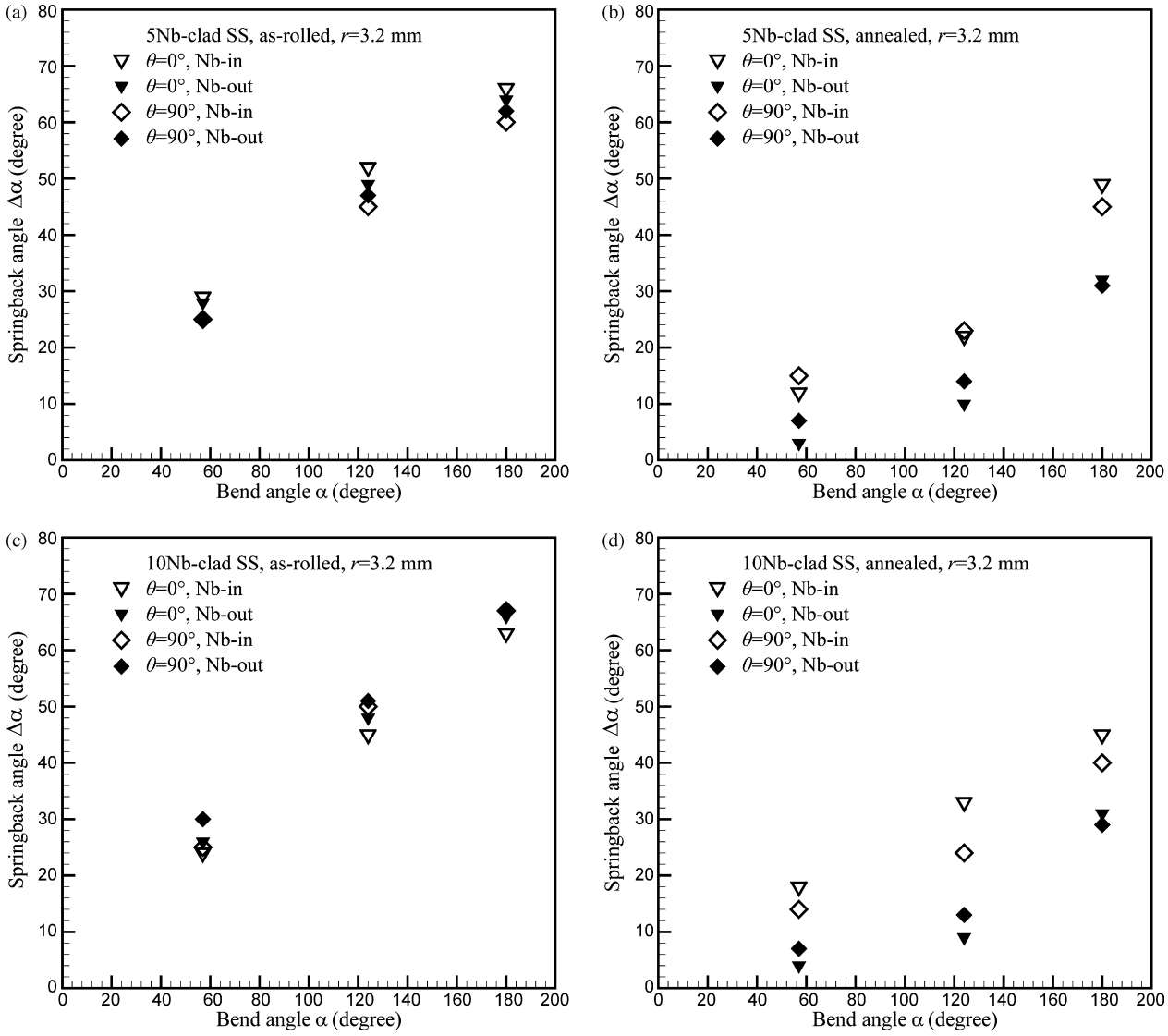


Fig. 5. Springback angle, Δα, as a function of the bend angle $\alpha$ (with $r = 3.2$ mm) for: (a) the as-rolled 5Nb-clad SS, (b) the annealed 5Nb-clad SS, (c) the as-rolled 10Nb-clad SS, and (d) the annealed 10Nb-clad SS. The measurement uncertainty of the springback angle is ±1°.

thick intermetallic layer exists along the entire interface between the Nb cladding and underlying SS core. Chemical analyses at the points indicated in Fig. 6(b) are given in Table 5. Specifically the results of point 3 in Fig. 6(a) and point 4 in Fig. 6(b) suggest that a chromium–nickel substituted form of the iron–niobium η-phase $Fe_2Nb_3$ [22] is likely the compound present at both interfaces. Elemental line scans of niobium, nickel, iron, and chromium across the clad/core interface shown in Fig. 6(c and d) confirm these results. Transition metal η-phase compounds are known to cause embrittlement problems in heat treated alloys and brazed or welded joints [23].

In the PEMFC application, the primary corrosion concern is failure of the Nb cladding, which would expose the SS core to the low pH environment of the cell. The chances of this happening are more likely when the Nb is placed under tensile stresses,

Table 4
Chemical analyses at the points indicated in Fig. 6(a)

| Points | Composition (at%) | | | | | |
|---|---|---|---|---|---|---|
| | Fe | Cr | Ni | Mn | Si | Nb |
| 1 | 69.74 | 18.93 | 9.19 | 1.98 | 0.46 | 0 |
| 2 | 69.77 | 18.60 | 9.79 | 1.84 | 0 | 0 |
| 3 | 39.95 | 9.32 | 4.09 | 0.87 | 0.63 | 45.14 |
| 4 | 1.20 | 0 | 0 | 0 | 0 | 98.80 |
| 5 | 0 | 0 | 0 | 0 | 0 | 100 |

Table 5
Chemical analyses at the points indicated in Fig. 6(b)

| Points | Composition (at%) | | | | | |
|---|---|---|---|---|---|---|
| | Fe | Cr | Ni | Mn | Si | Nb |
| 1 | 69.30 | 18.90 | 9.50 | 1.86 | 0.44 | 0 |
| 2 | 70.18 | 18.50 | 9.15 | 2.16 | 0 | 0 |
| 3 | 64.34 | 19.96 | 8.73 | 1.74 | 0 | 5.52 |
| 4 | 37.85 | 8.82 | 4.07 | 0 | 0.52 | 48.74 |
| 5 | 0.87 | 0 | 0 | 0 | 0 | 99.13 |
| 6 | 0 | 0 | 0 | 0 | 0 | 100 |

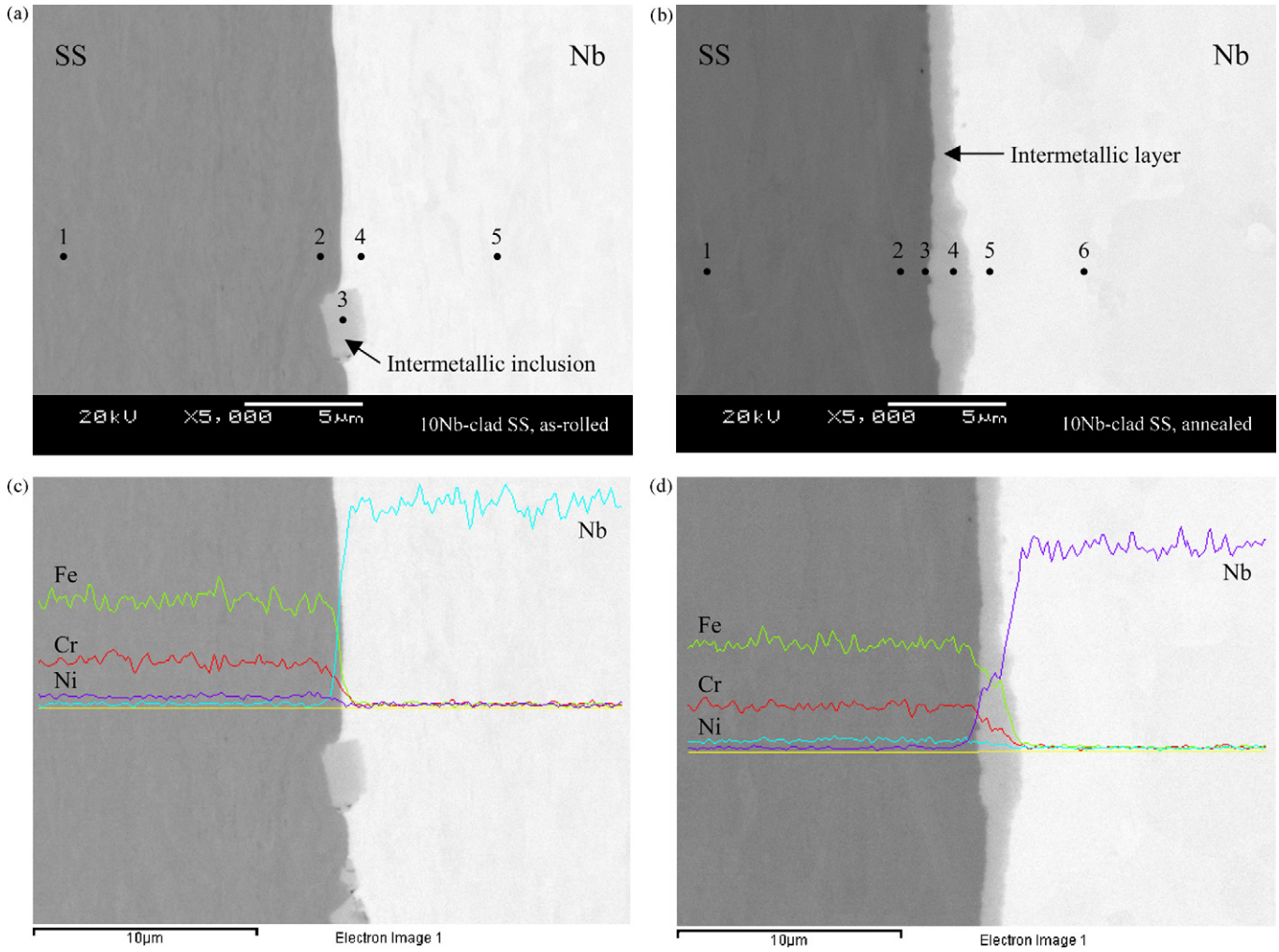


Fig. 6. Cross-sectional secondary electron images of: (a) the as-rolled and (b) annealed 10Nb-clad SS. Elemental line scans of niobium, nickel, iron, and chromium across the clad/core interface of (c) the as-rolled and (d) annealed 10Nb-clad SS.

i.e. when sheet bending occurs in the Nb-out orientation. Shown in Fig. 7(a and b) are cross-sectional optical micrographs of the 10Nb-clad SS specimens in the as-rolled and annealed conditions, respectively, after bending to $\alpha = 180^\circ$ ($r = 3.2$ mm) in the Nb-out orientation. It is apparent that neither sample exhibits surface or interfacial failure under these conditions. In general, none of the specimens listed in Table 1 that were tested to a maximum bend angle of 180° displayed any signs of failure or incipient failure during bend testing. However, when the specimens were then flattened, two different types of material failure were observed.

Shown in Fig. 8(a and b) are cross-sectional optical micrographs of the as-rolled and annealed 5Nb-clad SS specimens, respectively, after flattening in the Nb-out orientation. As seen in Fig. 8(a), the as-rolled specimen undergoes fracture localized at the bend tip due to low ductility. The cladding is cracked and peeled from the underlying SS core. In addition, the cracks extend into the core. The cracks observed inside the bend in Fig. 8(a) are likely due to tensile stresses induced by the springback of the as-rolled specimen during unloading. Similar observations were made in the as-rolled, Nb-in oriented specimens. On the other hand, the flattened annealed specimens do not crack, but instead undergo a ductile form of failure. As seen in Fig. 8(b), de-bonding begins to occur along the clad/core interface due to interfacial pore formation. Localized necking is apparent in the Nb layer near the bend tip, which in several places is sufficiently extensive to form through-thickness gaps in the cladding.

A higher magnification image of region A in Fig. 8(b) is shown in Fig. 9(a). It is clearly seen that the pores are found solely in the interfacial intermetallic layer, are periodically spaced ~5 μm apart, and have begun to grow into the adjacent Nb and SS layers. As shown schematically in Fig. 9(b–d), eventual failure of the Nb cladding in the Nb-out orientation is suspected to occur in stages as the imposed strain state in the material reaches a critical level. In the initial stage of bending, Fig. 9(b), none of the layers, clad, interfacial, or core, has reached a sufficiently high state of strain to cause imminent brittle fracture (in the intermetallic layer) or ductile necking (in the cladding layer). As bending progresses, Fig. 9(c), the strain within the intermetallic layer eventually reaches that required for brittle fracture, causing a series of cracks to form that essentially

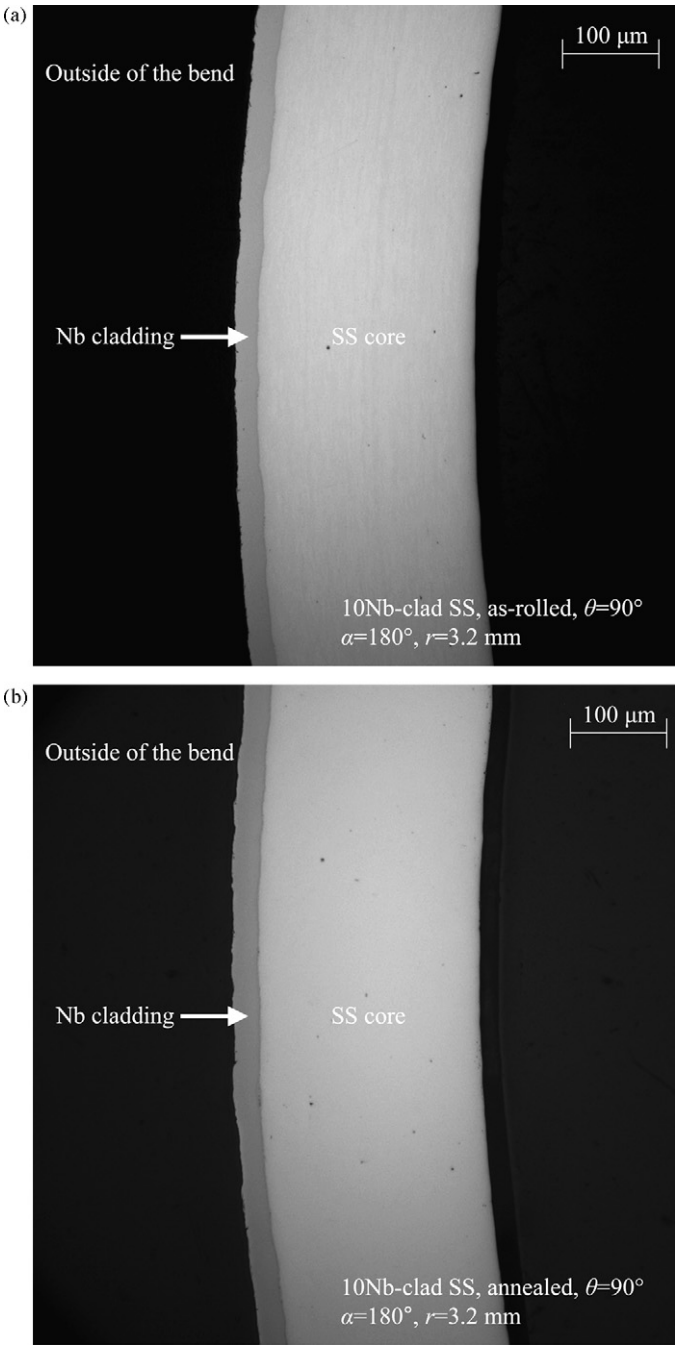


Fig. 7. Cross-sectional optical micrographs of the 10Nb-clad SS specimens in: (a) the as-rolled and (b) annealed conditions after bending to angle of $\alpha = 180^\circ$ ($r = 3.2$ mm) in the Nb-out orientation.

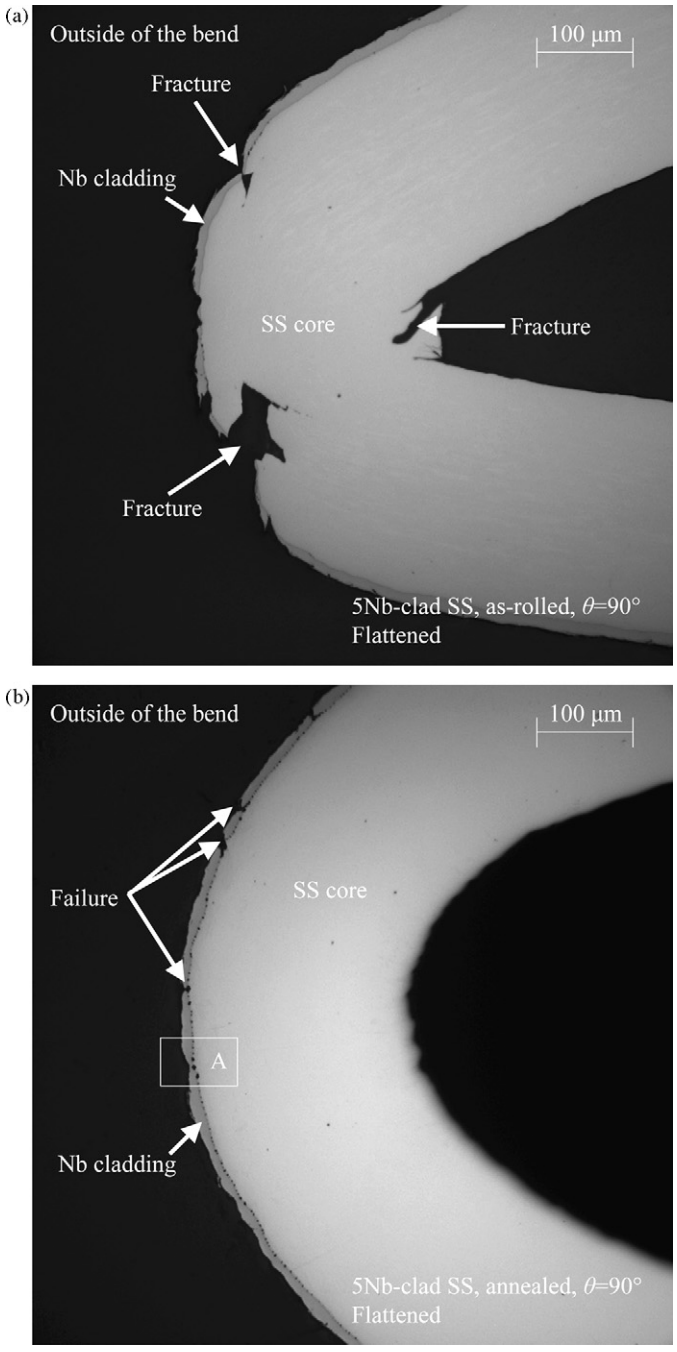


Fig. 8. Cross-sectional optical micrographs of: (a) the as-rolled and (b) annealed 5Nb-clad SS specimens after flattening in the Nb-out orientation.

relieve the stresses in this material. The flow stresses within Nb layer remain low enough that the imposed strain can be accommodated without necking. In the final stage of bending, Fig. 9(d), stress concentration begins to take place in both the Nb and SS materials at the tips of the cracks, causing an increasing level of plastic deformation to take place. With respect to the Nb layer, this induces localized straining or necking to occur and eventual through-thickness failure. The mechanism is similar to that reported by Matsumoto et al. [24] for annealed Al-clad Mg–Li alloy plate under bending.

Both brittle fracture of the work-hardened Nb layer in the as-rolled materials and ductile necking in the annealed clad metal sheets will negate the effectiveness of the protective cladding in the PEMFC bipolar plate application. Thus, it is important to understand the potential mechanical limitations applicable to the stamping, bending, and other forming operations that will be employed in fabricating the final clad metal plate. Results from the present study indicate that: (1) annealing is necessary to control the amount of springback that material displays during forming and to mitigate possible fracture in the cladding and (2) once annealed, the material can be bent extensively during

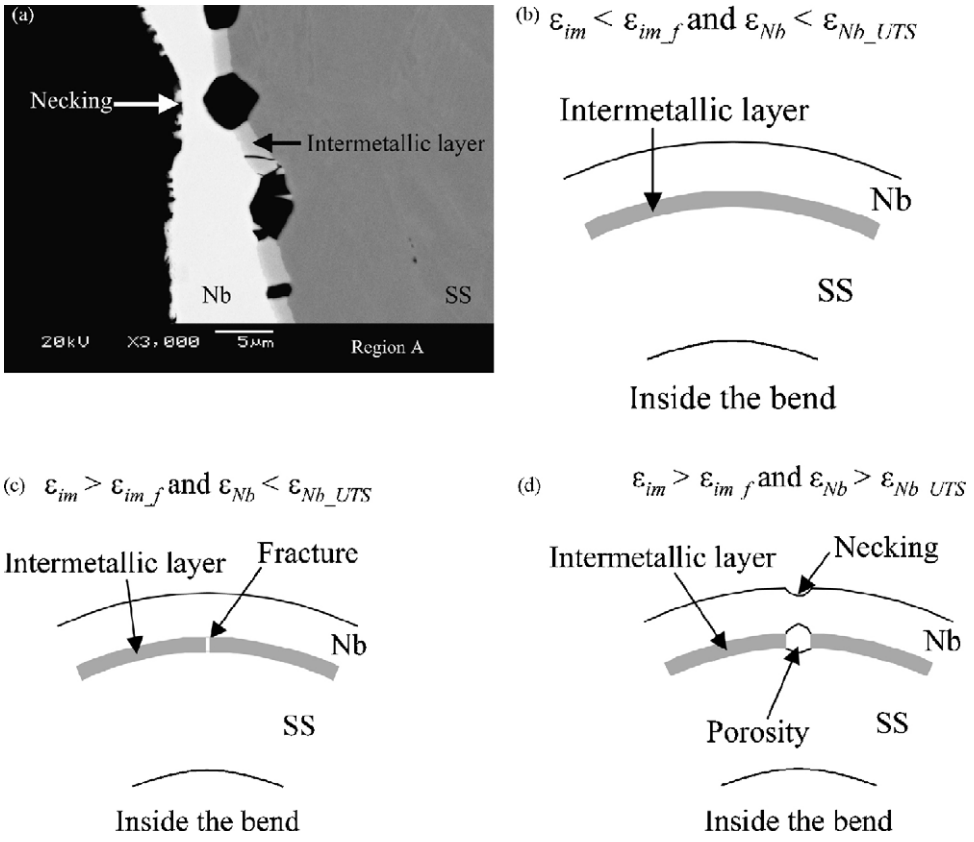


Fig. 9. (a) A secondary electron image of the region A in Fig. 8(b). (b–d) A schematic of the failure mechanism of the annealed specimen in the Nb-out orientation. (b) No failure occurs: none of the materials reaches the strains necessary for brittle fracture or necking. (c) The strain of the intermetallic layer reaches that required for fracture, while that in the cladding is sufficiently low that the Nb accommodates it without necking. (d) The cracks open forming pores between the Nb and SS layers and inducing localized necking in the Nb layer. Subscripts im, im_f, Nb, and Nb_UTS represents intermetallic layer, intermetallic layer at fracture, Nb layer, Nb layer at UTS, respectively.

stamping, however plate design features requiring complete flattening generally should be avoided. As a follow-up to this work, formability studies will be conducted on the annealed Nb-clad SS materials and the effects of sheet deformation on electrochemical properties will be examined via polarization testing and contact resistance measurements.

## 4. Conclusion

The quasi-static tensile test results indicate that annealing significantly improves the ductility of the Nb-clad 304L SS sheet material. Bend test results show that for the as-rolled material springback is essentially independent of bend direction and specimen orientation. The annealed specimens exhibit significantly less springback, the magnitude of which is dependent on whether the Nb cladding layer is in compression (i.e. on the inside of the bend) or in tension (i.e. on the outside of the bend). This dependency indicates that the asymmetry of the clad material exerts an appreciable effect on springback when the material has been softened via annealing. Microstructural analysis of the specimens indicates that depending on the original thermomechanical condition of the material two failure conditions can potentially occur, both under the extreme bending condition of flattening. Failure of the as-rolled material takes place via fracture through the work-hardened Nb cladding layer whereas that in the annealed material originates in an intermetallic layer that forms between the Nb and SS during the annealing process. Because this micron thick layer is brittle, it eventually fractures into a series of periodically spaced cracks that with further bending form pores which initiate necking and eventually through-thickness failure in the Nb cladding layer. These results suggest that annealing is required to induce sufficient ductility in the material that it can be plastically formed into a PEMFC bipolar plate. In addition, the flow channel dimensions of the plate should be designed to avoid extreme levels of strain at the cladding/core interface during stamping and thereby mitigate the potential for crack/pore formation within the material.

## Acknowledgements

The authors thank Steve Chang at Engineered Materials Solutions, Inc. for providing the clad materials and for his technical assistance on the study, Michael Dahl and Karl F. Mattlin for their help in conducting the quasi-static tensile tests, and Shelly Carlson and Jim Coleman for their assistance on the microscopy work. The authors also would like to thank Professors William F. Hosford and Jwo Pan at the University of Michigan for valuable

discussions. This work was supported by the U.S. Department of Energy, Office of Energy Efficiency, and Renewable Energy. The Pacific Northwest National Laboratory is operated by Battelle Memorial Institute for the United States Department of Energy (U.S. DOE) under Contract DE-AC06-76RLO 1830.

## References

[1] M. Lin, Y. Cheng, M. Lin, S. Yen, J. Power Sources 140 (2005) 346–349.
[2] Department of Materials Science and Metallurgy, University of Cambridge, DoITPoMS TLP – Fuel Cells – Proton Exchange Membrane Fuel Cells, available at http://www.msm.cam.ac.uk/doitpoms/tlplib/fuel-cells/low_temp_pem.php.
[3] U.S. Department of Energy, Hydrogen, Fuel Cells & Infrastructure Technologies Program Multi-Year Research, Development and Demonstration Plan (2003–2010), available at http://www.eere.energy.gov/hydrogenandfuelcells/mypp.
[4] X. Li, I. Sabir, Int. J. Hydrogen Energy 30 (2005) 359–371.
[5] A. Hermann, T. Chaudhuri, P. Spagnol, Int. J. Hydrogen Energy 30 (2005) 1297–1302.
[6] R. Hornung, G. Kappelt, J. Power Sources 72 (1998) 20–21.
[7] J. Scholta, B. Rohland, V. Trapp, U. Focken, J. Power Sources 84 (1999) 231–234.
[8] N. Cunningham, D. Guay, J.P. Dodelet, Y. Meng, A.R. Hlil, A.S. Hay, J. Electrochem. Soc. 149 (2002) A905–A911.
[9] D.P. Davies, P.L. Adcock, M. Turpin, S.J. Rowen, J. Appl. Electrochem. 30 (2000) 101–105.
[10] H. Wang, M.A. Sweikart, J.A. Turner, J. Power Sources 115 (2003) 243–251.
[11] V.V. Nikam, R.G. Reddy, J. Power Sources 152 (2005) 146–155.
[12] S.-J. Lee, C.-H. Huang, Y.-P. Chen, J. Mater. Process. Technol. 140 (2003) 688–693.
[13] M.P. Brady, K. Weisbrod, I. Paulauskas, R.A. Buchanan, K.L. More, H. Wang, M. Wilson, F. Garzon, L.R. Walker, Scr. Mater. 50 (2004) 1017–1022.
[14] J.C. McClure, S. Joseph, R. Chianelli, P. Pich, P.J. Sebastian, Int. J. Hydrogen Energy 20 (2005) 1339–1344.
[15] K.S. Weil, G. Xia, Z.G. Yang, J.Y. Kim, Int. J. Hydrogen Energy, in press.
[16] C. Gomes, O. Onipede, M. Lovell, J. Mater. Process. Technol. 159 (2005) 91–98.
[17] ASTM E8-04, American Society of Testing and Materials, Philadelphia, 2004.
[18] ASTM E290-97a, American Society of Testing and Materials, Philadelphia, 2004.
[19] S. Kalpakjian, Manufacturing Engineering Technology, third ed., Addison Wesley, Reading, 1995, pp. 459–464.
[20] W.F. Hosford, R.M. Caddell, Metal Forming, second ed., Prentice Hall, London, 1993, pp. 55–60, 258–261.
[21] Properties and Selection: Nonferrous Alloys and Special-Purpose Materials, in: ASM Handbook, vol. 2, ASM International, Metals Park, Ohio, 2004.
[22] C.G. Schön, J.A.S. Tenório, Intermetallics 4 (1996) 211–216.
[23] A.M. Russell, Adv. Eng. Mater. 5 (2003) 629–639.
[24] H. Matsumoto, S. Watanabe, S. Hanada, J. Mater. Process. Technol. 169 (2005) 9–15.